HHS Public Access

Author manuscript

Small. Author manuscript; available in PMC 2016 January 21.

Published in final edited form as:

Small. 2015 January 21; 11(3): 319–328. doi:10.1002/smll.201400765.

Functional nanovalves on protein-coated nanoparticles for *in vitro* and *in vivo* controlled drug delivery

Angela A. Hwang[#1], **Jie Lu**[#2], **Fuyuhiko Tamanoi**[2], and **Jeffrey I. Zink**[*,1]

[1] Department of Chemistry and Biochemistry, California NanoSystems Institute, Jonsson Comprehensive Cancer Center, University of California Los Angeles, Los Angeles, California, USA.

[2] Department of Microbiology, Immunology and Molecular Genetics, California NanoSystems Institute, Jonsson Comprehensive Cancer Center, University of California Los Angeles, Los Angeles, California, USA

[#] These authors contributed equally to this work.

Abstract

A multifunctional mesoporous drug delivery system that contains fluorescent imaging molecules, targeting proteins, and pH-sensitive nanovalves was developed and tested. Three nanovalve-MSN systems (NV-MSNs) with varied quantities of nanovalves on the surface were synthesized. These systems were characterized and tested to optimize the trade-off between coverage of nanovalves on the MSNs to effectively trap and deliver cargo, and the remaining underivatized silanol groups that can be used for protein attachments. The NV-MSN system that has satisfactory coverage for high loading and spare silanols was chosen, and transferrin (Tf) was integrated into the system. Abiotic studies were performed to test the operation of the nanovalve in the presence of the protein. In vitro studies were carried out to demonstrate the autonomous activation and function of the nanovalves in the system under biological conditions. Enhanced cellular uptake of the Tf-modified MSNs was seen using fluorescence microscopy and flow cytometry in MiaPaCa-2 cells. The MSNs were then tested using in SCID mice, which showed that both targeted and untargeted NV-MSN systems were fully functional to effectively deliver cargo. These new multifunctional nanoparticles serve proof of concept of nanovalve functionality in the presence of large proteins and demonstrate another dimension of MSN-based theranostic platforms.

Keywords

mesoporous silica nanoparticles; drug delivery; doxorubicin; transferrin; in vivo

[*] Corresponding author zink@chem.ucla.edu.

Supporting Information

Supporting Information is available from the Wiley Online Library or from the author.

1. Introduction

Mesoporous silica nanoparticles (MSNs) have shown great promise for biological applications as a drug delivery system because they are nontoxic, easily functionalized, and possess high surface areas.[1-4] MSNs are able to contain and protect therapeutic agents inside the mesopores when the pore openings are controlled by nanovalves. In addition, the exterior surface can simultaneously contain targeting ligands to enhance cellular nanocarrier internalization. Two different approaches for improving the therapeutic delivery of MSNs have been previously shown: mechanized pore control, and targeting ligands. With the diverse silane chemistries available, a variety of nanomachines can be covalently attached to MSNs. These mechanized MSNs are activated only upon a certain stimulus (light, enzyme, redox, magnetic field, pH) to remove the pore capping agent and enable the MSN contents to diffuse out, thereby achieving spatial and temporal control of the delivery of therapeutics.[5-7] pH-sensitive activation is of special interest as delivery can be autonomously activated *in vitro* and *in vivo*, due to the acidic conditions of the lysosomal compartments. These nanovalves remain closed at physiological pH (7.4), protecting and trapping the cargo. When the MSNs are endocytosed by cells and enter the lysosome (pH < 6), the pH-sensitive nanovalve will be activated— opening and releasing its contents to provide a stimulus-responsive and autonomous release of therapeutics. Many other MSN-based systems have applied pH-sensitivity to other pore-capping strategies, such as polymers, proteins, and peptides.[8-15]

Nanocarrier delivery can also be enhanced by derivatizing the MSN surface with biologically active targeting molecules (e.g. folate, RGD, transferrin) that increase the endocytosis of MSNs into cancer cells overexpressing receptors for such molecules.[16-19] These molecules incite biological responses from the cancer cell that increases NP endocytosis relative to their untargeted counterparts. Various cancer cell types express upregulated transferrin receptors (TfR) due to the higher iron requirement for cell proliferation.[20-22] Iron is carried into the cell by the 79 kD transmembrane protein, transferrin (Tf), which can be exploited to increase delivery payload of therapeutics and maintain a localized region of treatment. Our group as well as others have successfully shown the enhanced delivery of therapeutics by transferrin-modified nanoparticles that induce receptor-mediated endocytosis in cancer cells.[17, 23-28] We have demonstrated the enhanced delivery of delivery hydrophobic drugs (camptothecin, taxol) with the folate- and transferrin-modified MSNs, relying on the hydrophobic and hydrophilic forces to retain the hydrophobic cargo inside the MSN as it travels through the aqueous cellular media. However, if pore control and targeting functions can be integrated, we can fabricate a delivery system that synergistically delivers hydrophilic cargo in a localized and controlled manner.

In this paper, the design, fabrication, and operation of a multifunctional MSN delivery system that simultaneously contains fluorescent molecules, targeting proteins, and pH-sensitive nanovalves are presented. The nanovalves can autonomously activate and deliver hydrophilic cargo when exposed to a pH lower than 6 even in the presence of a 79 kD protein. The system is optimized and tested abiotically, demonstrating the successful operation of a nanovalve in the presence of the bulky targeting protein. The transferrin

protein slightly impedes the release of cargo, but *in vitro* testing with human pancreatic cancer cells (MiaPaCa-2) shows an enhanced delivery of doxorubicin (Dox) and cell killing. An *in vivo* study using SCID mice xenografts was subsequently carried out and showed successful delivery of Dox by using MSNs compared to that of the free drug. However, the transferrin targeting particles did not improve delivery compared to the untargeted particles because the impeded release of cargo counteracted the targeting.

2. Results and Discussion

2.1. Design, synthesis, and testing of pH-responsive nanovalves

In order to design a system that includes both targeting and pH-sensitive functionalities, a simple and sensitive nanovalve system that could be easily integrated into a well-established targeting scheme was chosen.[29] The nanovalve is composed of an aniline-based stalk that is grafted onto the surface of the nanoparticle, which forms an inclusion complex with α-cyclodextrin (α-CD) via hydrophilic and hydrophobic interactions to seal cargo inside the pores at neutral conditions. When exposed to acidic conditions, the phenyl amine is protonated ($pK_a \approx 6$) and the binding constant between the stalk and α-CD dramatically decreases, causing the cyclic sugar to de-bind and allow the cargo to diffuse out.

The first task was to optimize the nanovalve-MSN system in the presence of the targeting agent. There are a limited amount of silanol groups on the external surface of the MSNs, which made it necessary to adjust the relative surface coverage to simultaneously accommodate the nanovalve and a protein-coupling agent. Determining the appropriate amount of nanovalves necessary for sufficient pore capping and targeting was crucial in order for the two modalities to work synergistically. Therefore three different MSNs systems (Nanovalve-1, Nanovalve-2, Nanovalve-3) were synthesized that contained 50%, 85%, and 100% of the concentration for maximum surface coverage of nanovalves (**Scheme 1**). The nanovalves were grafted onto the surface via silanol exchange in dry toluene.

To confirm the nanovalve attachment and determine quantity of surface coverage, solid-state ^{13}C and ^{29}Si CPMAS NMR spectroscopy and thermogravimetric analysis were preformed. The ^{13}C CP/MAS SSNMR spectrum shows characteristic peaks in the aliphatic region from the propyl and methoxy groups, and four phenyl peaks in the aromatic region (**Figure S1**). Analysis of the ^{29}Si CP/MAS SSNMR spectrum show peaks in the T and Q regions, which are attributed to the silicon atoms in the bulk silica (Q region) and the silicon atoms from the surface-functionalized nanovalves (T region) (**Figure S2**). TGA showed the quantitative differences of the surface coverage, which confirmed the various quantities used in the synthesis of the nanovalve (NV-1, 6.98; NV-2, 7.82; NV-3, 8.27 % wt). As expected, the more thread used in the synthesis, the higher the weight percentage, and thus the greater number of nanovalves on the particle surface.

The new NV-MSN systems were loaded with doxorubicin (Dox), a water-soluble and widely used anticancer drug, to determine the behavior of the nanovalve as a function of surface coverage. Dox has a bright red fluorescence under laser stimulation (λ_{ex} = 480 nm; λ_{em} = 560-590 nm), which makes it convenient to detect in release experiments. After loading, the nanoparticles were capped with α-CD and the excess dye was washed away

with water until the supernatant was clear. Dox functions by inhibiting the progression of the enzyme topoisomerase II and can induce severe adverse effects such as life threatening heart damage. Many approaches to deliver Dox to target cancer cells in order to reduce its toxicity have been investigated, such as liposome-encapsulated forms Doxil, Caelyx, and Myocet.[30-31]

The three NV-MSN systems were tested abiotically using real-time continuously monitored fluorescence spectroscopy. To measure the amount of cargo that could be trapped by the different concentrations of nanovalves as well as to determine each sample's loading capacity, small amounts of dry Dox-loaded NV-MSNs were placed in a cuvette that was then filled with water. The fluorescence of the supernatant was monitored as a function of time before and after acidification. The initial flat baseline shows no increase of fluorescence (hour 0-1), indicating that the cap is tightly secured onto the stalk and there is no premature release of cargo **(Figure 3)**. The nanovalve is activated in the aqueous solution by adjusting the pH to 5.5, which causes the amine groups on the nanovalves to become protonated and thus decrease the binding constant between the stalk and α-CD. The bulky CD dissociates from the stalk and enables the cargo to diffuse out. The movement of the cargo from the particles into the bulk solution is quantified by monitoring the increase of fluorescence of the supernatant in real time. When each release was complete, an aliquot of the supernatant was removed and analyzed by UV-vis. The quantity of Dox released in the pH = 6 solution was calculated using Beer's law, and these data were later used to normalize the release profiles to one another. The release capacities were dependent on the quantity of surface functionalizations on the MSNs. The NV-3 had the highest release capacity of 1.2% wt, while NV-1 had the lowest (0.2% wt), and sample NV-2 had a release capacity of 0.5% wt.

The quantity of cargo released from the NV-MSNs was directly related to the extent of nanovalves on the surface and the rate was dependent on the amount of cargo released. In order to be effective at holding cargo, the nanovalves must block both ends of the hexagonal pore openings on the MSNs. As the surface coverage of nanovalve decreased, the loading capacity and release rate were lowered because there were fewer capped pore channels to hold cargo. The trend of release rate was NV-3 > NV-2 > NV-1, which corresponds to the relationship between nanovalve surface coverage and loading capacity of the MSN. Complete release of NV-1 is achieved in 3.5 hours, evidenced by the intensity. The profile of NV-2 begins to plateau at 5 hours, and the NV-3 sample still has a nonzero slope at hour 6. It can be concluded that the new NV-MSN systems work, but suffer consequences from decreased quantity of nanovalves on the surface. NV-2 has a release that is 20% less than that of the full coverage sample, but NV-1 is only about 35% (NV-3). The NV-2 MSN system was chosen to be the optimum value to be able to accommodate the Tf while maintaining a relatively large release capacity for cargo.

2.2. Integrating pH-responsive nanovalves and Tf targeting into MSN system

The targeting component was attached to the chosen NV-2-MSN system by functionalizing the particles with the thiol-terminated silane, 3-mercaptopropyltrimethoxysilane (MPTMS), to serve as the protein-coupling agent. The M-NV-MSNs were loaded with Dox and capped

before the protein was attached. Finally, transferrin (Tf) was covalently bonded to the nanoparticle by the thiol-disulfide exchange. The thiol-terminated particles are suspended in and added drop-wise to a protein solution and adjusted to a basic pH with $NaHCO_3$. Under basic conditions, the thiolate anion forms and exchanges readily with the disulfide bonds in the protein.[32] By attaching the Tf last, the denaturation of the protein is limited because the synthetic steps to attach the nanovalves would expose the protein to non-ideal conditions, such as nonpolar solvents and heat.

The assembled Tf-NV-MSNs were characterized by three methods. TEM imaging showed that the porous structure of the nanoparticle was preserved even after extensive surface modifications. Because electron microscopy cannot image small molecules or proteins on the particles' surface without staining, the apparent diameters of the nanoparticles did not appear to change after the surface modifications (**Figure S2**). Dynamic light scattering (DLS) was performed to ensure the nanoparticles were well suspended and monodisperse for biological studies. DLS showed the NV-MSN sample had an average hydrodynamic diameter of 108 nm, while the protein-modified MSN had a diameter of 117 nm (**Figure S3**). The increase in the average hydrodynamic radius (9 nm) is consistent with the addition of a protein (~ 6 nm) and the nanovalve on the surface of the MSN. Thermogravimetric analysis (TGA) shows the total surface coverage of both protein and assembled nanovalve was approximately 9% wt and degrades between temperatures 120 and 400 °C (**Figure S4**).

To verify the presence of Tf on the nanoparticles, a modified Bradford assay was preformed. Nanoparticles with and without protein modification were treated with the dye Comassie Brilliant Blue and the samples' supernatants were analyzed by UV/vis absorption spectroscopy. The dye primarily exists in its green form (λ_{max} = 650 nm), but will bind to the protein, shifting the dye to its a blue form (λ_{max} = 595 nm). The absorption spectrum of aqueous Comassie Brilliant Blue shows two peaks at 470 and 650 nm that are indicative of the two unbound forms, while the peak at 595 nm for its bound form is absent. Upon adding a suspension of Tf-MSNs, the solution turned blue and the absorption spectrum only exhibited a broad peak at 595 nm, diagnostic of the dye binding to protein (**Figure S5**). Moreover, the supernatant of the Tf-MSN solution was measured and there was a negligible amount of absorbance at 650 nm. As a control, unmodified MSNs were also assayed and did not exhibit any bound protein peaks in the spectrum. These data suggest that Tf proteins are on the MSNs and are not in solution.

In order to understand the behavior and operation of the nanovalve in the presence of the Tf protein, abiotic studies were performed using the aforementioned fluorescent spectroscopic technique. After the pH was adjusted to 5.5, the release profile Dox was obtained. Profiles of the MSNs with and without protein modification show successful release of Dox that confirm the nanovalves' operation with large proteins on the surface.

The two sets of nanoparticles show successful activation of the nanovalve with release of cargo and demonstrate different release kinetics as seen in **Figure 2B**. The Tf-modified NV-2-MSNs exhibit some impedance of cargo diffusion from the pores— the release rate at slightly acidic pH is considerably slower than that of the NV-2-MSNs. The cargo is not fully released even after 13 hours, which can be attributed to the protein delaying the diffusion of

the cap and cargo from the pores. The MSNs with only the nanovalve have a faster rate of release; 90% of the cargo is in the solution after 4 hours (Figure 2B, black trace). Because Dox is positively charged, the cargo can be electrostatically adsorbed to the surrounding proteins, slowing and hindering the diffusion process as the cargo leaves the pore. We have also observed a similar effect in samples with both polymer coatings and nanovalves on the silica surface.[33]

However there is a negligible difference in the overall loading capacities of both materials. Dox-loaded nanoparticles were treated with a strong acidic solution (pH = 1) to release the MSNs' entire contents. The solution was buffered back to neutral pH, the UV-vis absorption spectrum of the supernatant was measured, and the concentration of the drug was calculated via Beer's law. The Dox-loaded NV-MSNs have a loading capacity of 2.5 % wt, while the Tf-NV-MSNs have a loading capacity of 3.8 % wt (**Figure S7**). The loading capacity of the Tf-NV-MSNs is slightly higher, which can be attributed to the modified loading method that is used to protect the transferrin.

2.3. Enhanced Cellular Uptake of Tf-modified MSNs

After the MSNs were optimized as described above, *in vitro* studies were carried out to test the efficacy of the targeting agent in a pancreatic cancer cell line, MiaPaCa-2. The MSNs were synthesized and fluorescently labeled with fluorescein via a co-condensation method. Cells were incubated with MSNs with and without Tf modification for 24 hours, and subsequently washed with phosphate-buffered saline (PBS) solution to remove the excess MSNs. The cells were imaged via fluorescence microscopy, which showed that the MSNs (green fluorescence, fluorescein) were located within the cell (red fluorescence, WGA-Alexa Fluor 594 stain) (Figure 5A). The Tf modification on the cellular uptake resulted in enhanced uptake, shown qualitatively by the increase of cellular fluorescence by the Tf-targeted MSNs. Flow cytometry was performed to confirm and quantify the observed enhanced uptake of Tf-modified nanovalves inside the MiaPaCa-2 cells. As shown in **Figure 5B**, the amount of internalized Tf-MSNs is significantly higher than that of the MSNs without targeting agent. These results are explained by the overexpression of transferrin receptor (TfR) on the MiaPaCa-2 cancer cells, which facilitates the recognition and binding of the Tf-modified MSNs, thereby increasing the intracellular uptake.

2.4. Intracellular release of fluorescent dyes

The MSNs were loaded with fluorescent model cargo molecules to demonstrate the autonomous activation and function of the nanovalves in biological conditions, after the enhanced cellular uptake of Tf-modified MSNs was established. For this purpose two fluorescent dyes were used. Membrane impermeable propidium iodide (PI), and membrane permeable Hoechst 33342 (Hoe) were used as guest molecules in MSNs with and without the targeting protein. As PI is impermeable to lysosome membranes, it is unable to stain the cell nuclei if the nanovalves open inside the acidic lysosomes. Conversely, once Hoe is released, it can cross the lysosomal membrane easily and stain the nuclei. If PI is released into cytosol, it will stain the nuclei by intercalating into the DNA. Two cell lines (HFF, PANC-1) were cultured overnight with dye-loaded MSNs on a Lab-Tek chamber slide system (Nalgel Nunc International) to allow for cellular uptake, cargo release, and staining.

As shown in the Supplemental Information, the Hoechst dye was released and the cell nuclei were stained bright blue, for the both sets of MSNs (**Figure S6A)**. It should be noted that the Tf-NV-MSNs show a brighter staining that is indicative of enhanced uptake by targeting. Alternatively when PI is employed as cargo, there are no observable cell nuclei staining with the same length of treatment. Even though the acidic environment of the lysosomal compartments causes release of PI, all of the released PI molecules are confined in the lysosomes due to the membrane impermeable nature of PI.

It is also possible the observed nuclei staining with Hoechst-loaded MSNs simply might be due to leakage of dye from the pores before the cellular uptake even occurs. To rule out this possibility, MiaPaCa-2 cells were incubated with dye-loaded MSNs for 3 hours (Chamber 1); the supernatant was collected, and then used to treat cells in another chamber (Chamber 2) for 30 minutes before being subjected to fluorescence microscopic examination. If the dye had leaked from the MSNs before their cellular uptake, the dye should be in the supernatant and would be able to stain the cells in Chamber 2. In **Figure S6B**, the cells in Chamber 1 show brightly stained nuclei but there is no detectable staining in Chamber 2, proving that leakage is negligible.

These experiments prove that the NV-MSNs can release cargo in the lysosomes and stain the nuclei. However, the intracellular dye release observed is not necessarily due to the lower pH environment in the lysosomes; other unexpected stimuli could exist within a complex biological system. To prove the nanovalve activation is due to the acidic environment of the lysosome, the acidity of lysosomes was altered by using a proton inhibitor Bafilomycin A1 (Baf). Cells were treated with 160 nM Baf for 6 hours before the dye-loaded NV-MSNs were added to the cells. To examine the effect of Baf on the de-acidification of lysosomes, acridine orange (AO) staining was performed (**Figure 4**). AO is a fluorescent weak base that is frequently used as a probe for monitoring the acidification of organelles. In neutral or alkali environments it emits a green fluorescence, but when exposed to acidic compartments, it is ionized and it emits red light. In the untreated cells, red fluorescence was observed inside discrete cytoplasm organelles, indicating that the AO had accumulated in acidic organelles. However, the red fluorescence dramatically decreased after 6 hours of Baf treatment, indicating that the Baf had increased the pH of the lysosomes in the MiaPaCa-2 cells. NV-MSNs loaded with Hoechst dye were added to the cells and incubated for an additional 12 hours before examination by fluorescence microscopy. As shown in Figure 4, the treatment with Baf completely prevented the release of Hoechst from nanovalves, demonstrated by the lack of nuclear staining, as compared to the bright staining of the cells unexposed to Baf. This directly proves that the intracellular release of dye from MSNs was triggered by the acidity of the lysosomes.

2.5. Intracellular anticancer drug release from nanovalves

The previous experiments with fluorescent cargoes clearly demonstrate the pH-activated intracellular cargo release. To prove the synergistic cell killing effects of applying both pore control and targeted delivery, Dox was loaded into the NV-MSNs and tested in cancer cells. MiaPaCa-2 cells were incubated with fluorescein-labeled NV-MSNs for a range of 3 to 24 hours, washed with PBS, fixed with cold methanol, and examined by fluorescence

microscopy. The NV-MSNs (green fluorescence) incubated for 3 hours primarily co-localize with Dox (red fluorescence) and are distributed within lysosomes, primarily in the perinuclear areas (**Figure 5**). However after 12 hours of incubation, the red fluorescence of Dox no longer co-localized with green NV-MSNs but was observed in the nuclei. These images are is indicative of the drug exiting the lysosome and entering the nucleus, which is essential for the drug to be effective at cell killing.

Subsequently, the MSN systems were tested to determine if the Tf targeting agent and nanovalve functionalizations would deliver Dox more efficiently than with only the nanovalve on the surface. MiaPaCa-2 cells were treated with NV-MSNs (with and without transferrin) loaded with or without Dox for 72 hours. The cells that survived were counted with a WST-8 cell counting kit. **Figure 6** shows the MSNs modified with the nanovalve alone did not induce proliferation suppression to cells, while Dox-loaded NV-MSNs showed a significant cytotoxic effect even at very low concentrations (green trace). The Tf-NV-MSNs (blue trace) were even more effective at increasing cell cytotoxicity. The nanovalve is able to autonomously open and deliver Dox in the presence of the bulky protein, while transferrin is increasing the cellular uptake of the MSNs to focus its delivery. These data demonstrate the synergistic effects at work to deliver cargo more effectively.

2.6. *In vivo* anticancer effect of doxorubicin-loaded nanovalves

Successful in the *in vitro* model, the MSN system was tested in an *in vivo* model to understand the effectiveness of the nanovalve and targeting functions in an animal model. To establish human cancer xenografts, 5×10^6 MiaPaCa-2 cells were subcutaneously injected into the right lateral abdominal wall of the SCID mice. Mice were randomly divided into the treatment groups in each experiment after the tumors approximately 3 mm in diameter were palpable. Four mice bearing subcutaneous tumors approximately 8 mm in diameter were injected via tail vein with Dox-loaded MSNs, suspended in saline solution. After 4 and 24 hours, the mice were anesthetized, placed in the chamber of a Maestro 2 *in vivo* imaging system, and optic light and green fluorescent images were obtained. As shown in **Figure 7A**, a strong green fluorescence signal was detected in tumors of the mice treated with MSNs at 4 hours and 24 hours after the injection, indicating the accumulation of nanoparticles in tumors. After euthanasia, the tumors were collected and all tissues were analyzed by fluorescence imaging. The red fluorescence signal was observed from the tumors in the mice treated with Dox-loaded MSNs, but no signal was observed in mice treated unloaded MSNs (**Figure 7B**).

Next, 25 SCID mice with established xenografts of MiaPaCa-2 were randomly divided into 5 groups (n=5), and intraperitoneal injections of MSN solutions began after the average tumor diameter reached 3 mm (14^{th} day after inoculation). Animals in the first group received saline solution as control, Group 2 was treated with free Dox, Group 3 was treated with unloaded NV-MSNs, Group 4 was treated with NV-MSNs loaded with Dox, and Group 5 was treated with Tf-NV-MSNs loaded with Dox (the final concentrations of Dox were the same as Group 2). All injections were done twice per week until the end of the experiment (the 28^{th} day). The average body weights are unchanged, which shows that there is no significant toxicity of MSN systems to the mice **(Figure S7)**.

The tumors in the control group (Group 1) and unloaded NV-MSN group (Group 3) kept growing—showing the MSNs themselves did not affect the tumor growth in mice (**Figure 7C**). Tumor growth inhibition was significant with the administration of free Dox (Group 2). The mice treated with Dox-loaded NV-MSNs (Group 4) and Dox-loaded Tf-NV-MSNPs delivered to the mice in Group 5 also showed significant tumor suppression, demonstrating the effective autonomous delivery of Dox inside the tumor. Targeting effects are negligible, as the average tumor volume is within the statistical error of the untargeted MSNs. The results of the hematology and serology examinations are summarized in Table 1 (**Figure S8**). The blood test from the mice of Group 2 and 4 showed mild bone marrow suppression without significant alteration of liver function or renal functions, which indicates the safety of the whole experiment.

These *in vivo* experiments demonstrate that the nanovalve-modified MSNs are adept at trapping and autonomously releasing cargo in xenograft tumors. The similarity between the therapeutic efficacies of the targeted and untargeted nanoparticles suggests complex *in vivo* effects. Possibilities include a simple screening effect in which local proteins block the transferrin protein from being sensed by the Tf receptors of cancer cells, or complex interactions with blood cells, such as erythrocytes and macrophages, that can prevent the Tf-NV-MSNs from reaching the tumor site and passing through intraepithelial gap of capillaries in the tumors.[34] Another possible explanation is that two competing effects are at play: the active targeting of the protein and the delayed release of cargo (Figure 4C). As previously discussed, it is probable that the targeting is active, but the impeded release greatly reduces the delivery of cargo and its efficacy. Further *in vivo* studies are necessary to evaluate the exact nature of this phenomenon in order to optimize the effect of transferrin targeting to enhance tumor shrinkage. This study demonstrates that both types of pH-sensitive MSNs are more effective for *in vivo* delivery of doxorubicin than the free drug counterpart.

3. Conclusion

In summary, we have designed and optimized a multifunctional MSN system that has demonstrated the operation of a pH-sensitive nanovalve in conjunction with transferrin as a targeting agent. Abiotic studies of the MSN system show efficient loading and pH-activated release of doxorubicin in the presence of the large Tf protein, and the release profiles demonstrate that the release kinetics are slower than that of MSNs without the protein. Cellular studies prove that the delivery of cargo is due to the pH activation of the nanovalves in the acidic lysosomes. Fluorescence microscopy images show that membrane permeable cargo can stain the nuclei, while cargo that is membrane impermeable remains in the endosome. The activation of the nanovalve is due to the acidic nature of the endosome—treatment of Baf to prevent the acidification of the lysosomal also prevents valve opening and cargo release. The cell cytotoxicity assays show the MSN delivery of Dox is more effective than free drug, and targeting by Tf increases its efficacy, especially at low concentrations. *In vivo* studies were carried out to demonstrate the effective pH-responsive MSNs in SCID mice. The effect of targeting was negligible, which can be attributed to the phenomena of delayed delivery or local proteins shielding the effect of transferrin in the body. To our knowledge, this is the first operation of a pH-sensitive nanovalve-MSN system

in vivo.[35] This study demonstrates that autonomously operating nanovalves function as designed in the presence of a bulky protein targeting agent not only in solution, but also in vitro and in vivo models.

4. Experimental Section

Materials

All reagents were used as received without further purification. 3-Aminopropyltriethoxysilane (APTES, 99%), *p*-anisidine (≥ 99%), cetyltrimethylammonium bromide (CTAB, 90%), α-cyclodextrin (α-CD, 98%), doxorubicin (98%), fluorescein isothiocyanate (FITC, 90%), bisBenzimide H 33342 trihydrochloride (Hoechst 33342, ≥90%), 4-(2-hydroxyethyl)-1-piperazineethanesulfonic acid (HEPES buffer, 0.05 M), propidium iodide (PI, 95%), tetraethyl orthosilicate (TEOS, 90%), transferrin (Tf, ≥98%) and 3-(trihydroxysilyl)propyl methylphosphonate monosodium aqueous solution (HTMP, 42%) were purchased from Sigma. 3-Iodopropyltrimethoxysilane (IPTMS, 90%) and 3-mercaptopropyltrimethoxysilane (MPTMS, 90%) was obtained from Gelest. Triethylamine (99.5%, EMD), ethanol (200 proof, Pharmaco-AAPER)

General Methods

Transmission electron microscopy (TEM) images were obtained using a JEM1200-EX (JEOL) instrument. UV-vis spectra were collected by a Cary 500 UV-vis-NIR spectrophotometer. The fluorescence release profiles were recorded by an Acton Spectra Pro 2300i CCD and excited by a CUBE 445-40C (Coherent Inc., Santa Clara, CA, USA) laser. ^{13}C CPMAS NMR spectra were obtained by a Bruker DSX-300 MHz Spectrometer with a 4 mm double resonance Bruker probe head, used with Zirconium oxide 4 mm rotors and Kel-F caps. Thermogravimetric analysis (TGA) was performed by a Pyris Diamond TG/DTA (Perkin-Elmer Instruments). DLS and zeta potentials were measured by ZetaSizer Nano (Malvern Instruments Ltd., Worcestershire, U.K.).

Synthesis of MSNs

An aqueous solution of CTAB (0.25 g, 0.7 mmol) and NaOH (875 μL, 2 M) was heated to 80 °C. TEOS (1.2 mL) was added to the ethanolic solution, and then added to the heated solution drop-wise. After waiting 20 minutes, 300 μL of HTMP was slowly added into the solution and aged for 2 hours. Once the solution was cooled, MSNs were collected by centrifugation, and washed with methanol. The surfactant was removed by refluxing in an acidic methanol solution overnight, washed with MeOH, and subsequently resuspended in the desired solvent. To fluorescently label the MSNs, a separate flask containing FITC (3 mg), APTES (6 μL), and ethanol (dry, 1.5 mL) was reacted under nitrogen for 2 hours. This solution was added to the TEOS prior to being condensed in the hot CTAB solution.

Surface Functionalizations

The nanovalves and protein-coupling agent were covalently attached to the surface of the MSNs by refluxing the silanes and MSNs overnight in dry toluene. In order to synthesize the nanovalve, MSNs were first derivatized with 3-iodopropyltrimethoxysilane and subsequently coupled to *p*-anisidine. For the three nanovalves systems (Nanovalve-1,

Nanovalve-2, and Nanovalve-3), differing quantities (15 μL, 25 μL, 30 μL, respectively) of IPTMS were used for 100 mg of MSNs in 10 mL of toluene. The solution was cooled and washed with additional aliquots of toluene. The iodo-functionalized NV-2 MSNs were then suspended in 10 mL of dry toluene and refluxed overnight with *p*-anisidine (120 mg) in the presence of triethylamine (450 μL). The NV-MSNs were consequently scaled with respect to the quantity of IPTMS. Again the solution was cooled and washed with toluene to remove unreacted materials. To prepare for the protein attachment, the NV-MSNs (100 mg) were subsequently modified with the MPTMS (7 μL) by refluxing overnight in toluene (10 mL) and washed with toluene, methanol, and suspended in water. TGA and solid state NMR confirmed the surface functionalizations.

Cargo Loading and Capping

Cargos (Hoechst, PI, Dox) were loaded into the MSNs by suspending 25 mg of MSNs in a concentrated solution (Hoe and PI: 1 mM, Dox: 4 mg/mL) and left to stir overnight. The nanoparticles were capped by adding α-CD (50 mg) and stirred for 24 hours. The MSNs that did not require any further modifications were thoroughly washed with water until the supernatant ran clear. MSNs that needed Tf-modification were washed only twice to prevent any loss of cargo by excessive washing.

Protein Attachment

Transferrin was covalently attached to the surface of the loaded and capped mercapto-modified NV-MSNs (M-NV-MSNs) by first suspending 25 mg in 1 mL of water. The suspension of nanoparticles was slowly added drop wise to a stirring solution of transferrin and HEPES buffer (1 mg/mL). Finally a 0.8 M $NaHCO_3$ (0.4 mL) was added for the reaction to proceed. The solution was capped and sealed in foil to prevent light exposure, and let stir for 4 hours at room temperature. The Tf-MSNs were carefully collected by centrifugation and washed several times with HEPES. To confirm the protein was on the nanoparticle, a modified Comassie assay was preformed and analyzed by absorption spectroscopy. Comassie blue typically absorbs at 595 nm, but will shift to 650 nm when exposed to protein. The suspension of Tf-MSNs absorbed at 650 nm but the measurement of the supernatant did not, indicating the Tf is on the MSN and not just in solution. The absorption spectra of the supernatant and suspension of MSNs with the Comassie assay were not red-shifted.

Abiotic Studies

To confirm the function and operation of the nanovalves, aqueous release studies were preformed on the MNSP systems. Samples loaded with cargo (5 mg) were carefully placed in the corner of a cuvette and filled with water (7 mL). A probe beam (448 nm) was used to excite the emission of the cargo being released in the bulk water and its fluorescence was continuously monitored by a spectrophotometer in real time. Once a flat baseline was obtained to show no leakage, the solution was adjusted to a pH of 5.5 to activate the acid-sensitive nanovalves. The supernatant of the solution was measured by UV-vis spectroscopy to calculate the loading capacity and to normalize the different release profiles.

Cell culture

Human cancer cells, MiaPaCa-2, were obtained from the American Type Culture Collection and were maintained in Dulbecco's modified Eagle's medium (DMEM) (GIBCO) supplemented with 10% fetal calf serum (Sigma, MO), 2% L-glutamine, 1% penicillin, and 1% streptomycin stock solutions. The media were routinely changed every 3 days, and the cells were passaged by trypsinization before confluence.

Microscopy

The MNSPs emit a green fluorescence when excited at 470 nm because of fluorescein (FITC) dye co-condensed within the silica matrix. Acridine Orange (AO) was used to monitor the acidic intracellular organelles. Cells were cultured on a Lab-Tek chamber slide system (Nalge Nunc International) overnight. After being incubated with MSNs for 3 hrs, the cells were washed with PBS, and incubated with 6 μMAO for 1 hr in DMEM without phenol red and washed with PBS, then examined with confocal microscopy (λ_{ex} = 470 nm) (Carl Zeiss LSM 310 Laser Scanning Confocal microscope). The cellular uptake and subcellular distribution of Doxorubicin-loaded nanovalves can be easily monitored using fluorescence microscopy since Dox exhibits bright red fluorescence under laser stimulation (excitation at 480 nm; emission maximum at 560-590 nm). MiaPaCa-2 cells were incubated with either Dox-loaded NV-MSNs or NV-MSNs for 3 hours or 12 hours at 37 °C and the fluorescence distribution was examined using a fluorescent microscope.

Cell Death Assay

The cytotoxicity assay was performed using a cell counting kit from Dojindo Molecular Technologies, Inc. Briefly, cancer cells were seeded in 96-well plates (5000 cells/well) and incubated in fresh culture medium at 37 °C in a 5% CO_2/95% air atmosphere for 24 hours. The cells were then washed with PBS, and the medium was changed to a fresh medium with indicated NV-MSNs at indicated concentrations. After the indicated incubation period, the cells were washed again with PBS. Then, 10% WST-8 solution in 100 μl of DMEM was added to the wells, and incubated for another 2 hours. Finally, the absorbance of each well was measured at 450 nm with a plate reader. Since the absorbance is proportional to the number of viable cells in the medium, the viable cell number was determined using a previously prepared calibration curve (Dojindo Co.).

Flow Cytometry

Flow cytometric analysis was used to detect the fluorescent signal of MSNs internalized by human cells. The cells treated with MSNs for 24 hours were collected, washed with PBS, and analyzed with a fluorescence-activated cell sorter (Caliber, Becton Dickinson).

Human Cancer Xenograft Establishment

5×10^6 human pancreatic cancer cells, MiaPaCa-2, collected in 0.2 mL DMEM, were s.c. injected into the right lateral back of the SCID mice (Charles River). Mice were randomly divided into treatment or vehicle groups in each experiment after the tumors of approximate 3 mm in diameter were palpable.

Biodistribution of NV-MSNs

4 SCID mice bearing subcutaneous tumors approximately 8 mm in diameter were injected via the tail vein with NV-MSNs loaded with doxorubicin suspended in saline solution. After 4 hours and 24 hours, the mice were anesthetized, placed in the chamber of a Maestro 2 *in vivo* imaging system (CRi, MA), and optic light and green fluorescent images were obtained. After euthanasia with CO_2, the tumors were collected, embedded, frozen, processed to 4 μm slides by our Tissue Processing Core Lab (TPCL, UCLA). All slides were then analyzed under a fluorescent microscope.

In Vivo Tumor Growth Assay

25 SCID mice with established xenografts of MiaPaCa-2 were randomly divided to 5 groups (n=5), and the intraperitoneal injections (0.5 mg/0.2 mL per mouse) began when the average tumor diameter reached 3 mm (14^{th} day after inoculation). Animals in the first group received saline solution as control (Group 1). Group 2 was treated with Dox only. Group 3 was treated with plain NV-MSNs without loading. Group 4 was treated with NV-MSNs loaded with doxorubicin (the final concentration of Dox is the same as Group 2). Group 5 was treated with Tf-NV-MSNs loaded with Dox. All injections were performed twice per week until the end of the experiment (the 28^{h} day). Tumor volume and body weight were monitored every other day, and tumor volume was calculated using the following formula: tumor volume = (4 / 3) × 3.14 × (L / 2 × W / 2 × W / 2), where L is the length and W is the width of the tumor. At the final day, all mice were sacrificed and subjected to autopsy. Blood was collected for serological and hematological examination, and the organs were analyzed by a pathologist for histopathological examination.

Statistical Analysis

All results are expressed as means ± SD. Statistical comparisons were made using Student's t test after analysis of variance. The results were considered to be significantly different at P value <0.05.

Supplementary Material

Refer to Web version on PubMed Central for supplementary material.

Acknowledgements

This research was supported by the NIH ROI CA133697 and by the Defense Threat Reduction Agency HDTRA1-13-1-0046.

References

1. a Argyo C, Weiss V, Bräuchle C, Bein T. Chem. Mater. 2013; 26:435–451. For reviews. b Ambrogio MW, Thomas CR, Zhao Y-L, Zink JI, Stoddart JF. Acc. Chem. Res. 2011; 44:903–913. [PubMed: 21675720] c Angelos S, Liong M, Choi E, Zink JI. Chem. Eng. J. 2008; 137:4–13.d Li Z, Barnes JC, Bosoy A, Stoddart JF, Zink JI. Chem. Soc. Rev. 2012; 41:2590–2605. [PubMed: 22216418] e Tarn D, Ashley CE, Xue M, Carnes EC, Zink JI, Brinker CJ. Acc. Chem. Res. 2013; 46:792–801. [PubMed: 23387478] f Trewyn BG, Slowing II, Giri S, Chen H-T, Lin VS-Y. Acc. Chem. Res. 2007; 40:846–853. [PubMed: 17645305] g Wu S-H, Mou C-Y, Lin H-P. Chem. Soc. Rev. 2013; 42:3862–75. [PubMed: 23403864]

2. Liong M, Lu J, Kovochich M, Xia T, Ruehm SG, Nel AE, Tamanoi F, Zink JI. ACS Nano. 2008; 2:889–896. [PubMed: 19206485]
3. Lu J, Liong M, Li Z, Zink JI, Tamanoi F. Small. 2010; 6:1794–1805. [PubMed: 20623530]
4. He Q, Shi J. Adv. Mater. 2013:1–21.
5. Lu J, Choi E, Tamanoi F, Zink JI. Small. 2008; 4:421–426. [PubMed: 18383576]
6. Thomas CR, Ferris DP, Lee J-H, Choi E, Cho MH, Kim ES, Stoddart JF, Shin J-S, Cheon J, Zink JI. J. Am. Chem. Soc. 2010; 132:10623–5. [PubMed: 20681678]
7. Meng H, Xue M, Xia T, Zhao Y-L, Tamanoi F, Stoddart JF, Zink JI, Nel AE. J. Am. Chem. Soc. 2010; 132:12690–7. [PubMed: 20718462]
8. Zheng Q, Lin T, Wu H, Guo L, Ye P, Hao Y, Guo Q, Jiang J, Fu F, Chen G. Int. J. Pharm. 2014; 463:22–26. [PubMed: 24393764]
9. Chen X, Cheng X, Soeriyadi AH, Sagnella SM, Lu X, Scott J. a. Lowe SB, Kavallaris M, Gooding J. J. Biomater. Sci. 2014; 2:121.
10. Cui Y, Xu Q, Chow PK-H, Wang D, Wang C-H. Transferrin-Conjugated Biomaterials. 2013; 34:8511–8520. [PubMed: 23932498]
11. Li C, Yang D, Ma P, Chen Y, Wu Y, Hou Z, Dai Y, Zhao J, Sui C, Lin J. Small. 2013; 9:4150–4159. [PubMed: 23843254]
12. Luo Z, Cai K, Hu Y, Zhang B, Xu D. Adv. Healthc. Mater. 2012; 1:321–325. [PubMed: 23184747]
13. Popat A, Liu J, Lu G. Q. (Max), Qiao SZ. J. Mater. Chem. 2012; 22:11173.
14. Zhang Q, Wang X, Li P-Z, Nguyen KT, Wang X-J, Luo Z, Zhang H, Tan NS, Zhao Y. Adv. Funct. Mater. 2013:1–12.
15. Zhao Z, Meng H, Wang N, Donovan MJ, Fu T, You M, Chen Z, Zhang X, Tan W. Angew. Chem. Int. Ed. Engl. 2013; 52:7487–7491. [PubMed: 23757374]
16. Lu J, Li Z, Zink JI, Tamanoi F. Nanomedicine. 2011; 8:212–220. [PubMed: 21703996]
17. Ferris DP, Lu J, Gothard C, Yanes R, Thomas CR, Olsen J-C, Stoddart JF, Tamanoi F, Zink JI. Small. 2011; 7:1816–26. [PubMed: 21595023]
18. Gao F, Li L, Liu T, Hao N, Liu H, Tan L, Li H, Huang X, Peng B, Yan C, Yang L, Wu X, Chen D, Tang F. Nanoscale. 2012; 4:3365–72. [PubMed: 22538830]
19. Mackowiak SA, Schmidt A, Weiss V, Argyo C, Schirnding C, von; Bein T, Bräuchle C. Nano Lett. 2013; 13:2576–2583. [PubMed: 23662711]
20. Inoue T, Cavanaugh PG, Steck PA, Brünner N, Nicolson GL. J. Cell. Physiol. 1993; 156:212–7. [PubMed: 8314858]
21. Heer HN, Kozlowski JM, Tsai YC, Lee C, McEwan RN, Grayhack JT. J. Urol. 1990; 143:2, 381–5.
22. Ryschich E, Huszty G, Knaebel HP, Hartel M, Büchler MW, Schmidt J. Eur. J. Cancer. 2004; 40:1418–22. [PubMed: 15177502]
23. Fang W, Wang Z, Zong S, Chen H, Zhu D, Zhong Y, Cui Y. Biosens. Bioelectron. 2014; 57C:10–15. [PubMed: 24525050]
24. Li H, Sun H, Qian ZM. Tren. Pharm. Sci. 2002; 23:206.
25. Yhee JY, Lee SJ, Lee S, Song S, Min HS, Kang S-W, Son S, Jeong SY, Kwon IC, Kim SH, Kim K. Bioconjug. Chem. 2013; 24:1850–60. [PubMed: 24107100]
26. Liu H, Liu T, Wu X, Li L, Tan L, Chen D, Tang F. Adv. Mater. 2012; 24:755–61. [PubMed: 22213059]
27. Liu G, Mao J, Jiang Z, Sun T, Hu Y, Jiang Z, Zhang C, Dong J, Huang Q, Lan Q. Cancer Biother. Radiopharm. 2013; 28:691–6. [PubMed: 23786401]
28. Shah N, Chaudhari K, Dantuluri P, Murthy RSR, Das SJ. Drug Target. 2009; 17:533–42.
29. Du L, Liao S, Khatib HA, Stoddart JF, Zink JI. J. Am. Chem. Soc. 2009; 131:15136–42. [PubMed: 19799420]
30. Mross K, Niemann B, Massing U, Drevs J, Unger C, Bhamra R, Swenson CE. Cancer Chemother. Pharmacol. 2004; 54:514–24. [PubMed: 15322827]
31. Gabizon AA. Cancer Invest. 2001; 19:424–36. [PubMed: 11405181]
32. Fava A, Iliceto A, Camera EJ. Am. Chem. Soc. 1957; 79:833–838.

33. Dong J, Xue M, Zink JI. Nanoscale. 2013; 5:10300–6. [PubMed: 24056925]
34. Salvati A, Pitek AS, Monopoli MP, Prapainop K, Bombelli FB, Hristov DR, Kelly PM, Åberg C, Mahon E, Dawson KA. Nat. Nanotechnol. 2013; 8:137–143. [PubMed: 23334168]
35. Chen Y, Chen H, Shi J. Adv. Mater. 2013; 25:3144–76. [PubMed: 23681931]

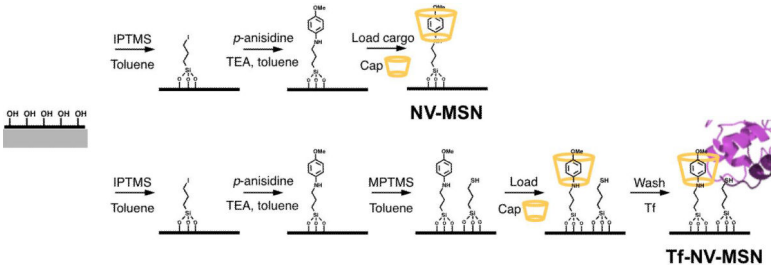

Scheme 1.

Synthetic schemes of acid valve assembly and incorporation of targeting agent. NVMSN denote particles that are modified with nanovalve only, and Tf-NV-MSN are particles that have both transferrin and nanovalve derivatizations.

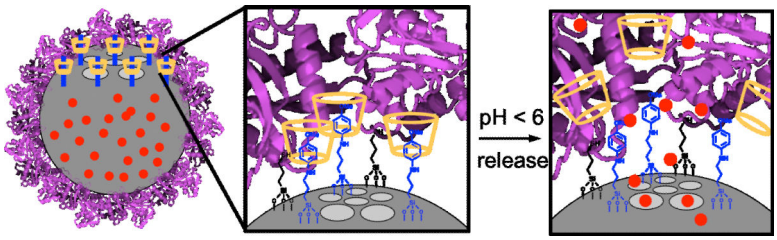

Figure 1.

Depiction of fully assembled Tf-NV MSN system: when the pH is adjusted to below 6, the nanovalves open, and the MSNs' contents diffuse out in the presence of transferrin.

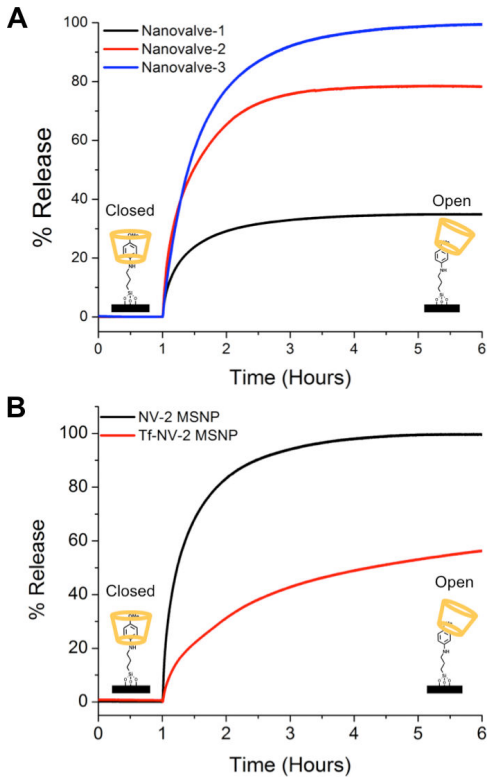

Figure 2.

a) Release profiles for particles with 50%, 85%, and 100% acid nanovalve surface coverage (respectively NV-1, NV-2, and NV-3). Capacity is dependent on the amount of surface coverage to hold cargo. b) Release of NV-2 MSN delivery systems with and without protein modification. Protein presence hinders release of cargo. All pH activations are performed at pH of 5.

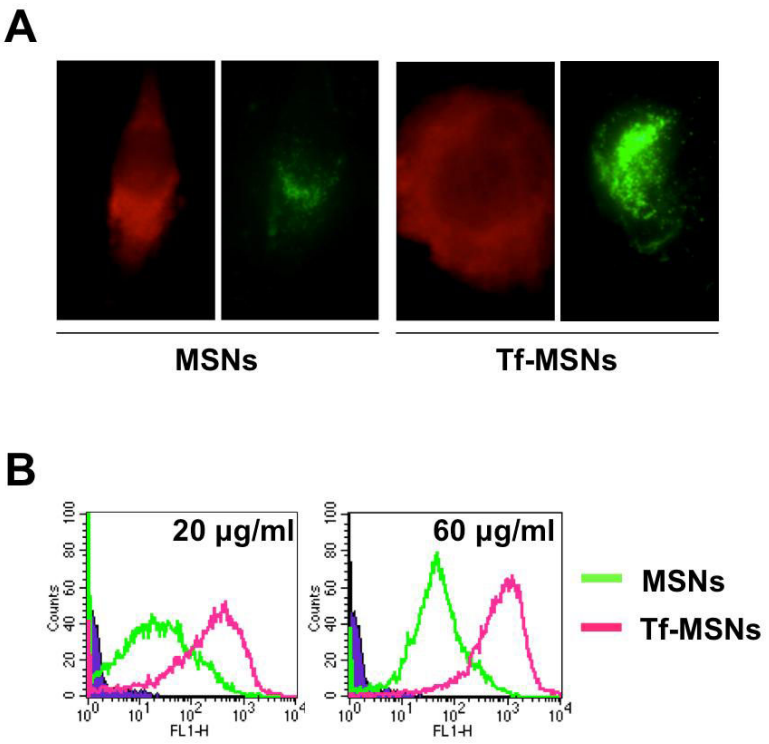

Figure 3.

a) Fluorescence microscopy images of cell (red) and MSNs (green) show increased fluorescence of the Tf-MSNs than the untargeted MSN, indicative of higher endocytosis of Tf-MSN; and b) Flow cytometry of targeted and untargeted MSNs at two different concentrations show Tf-MSNs have a significantly higher uptake.

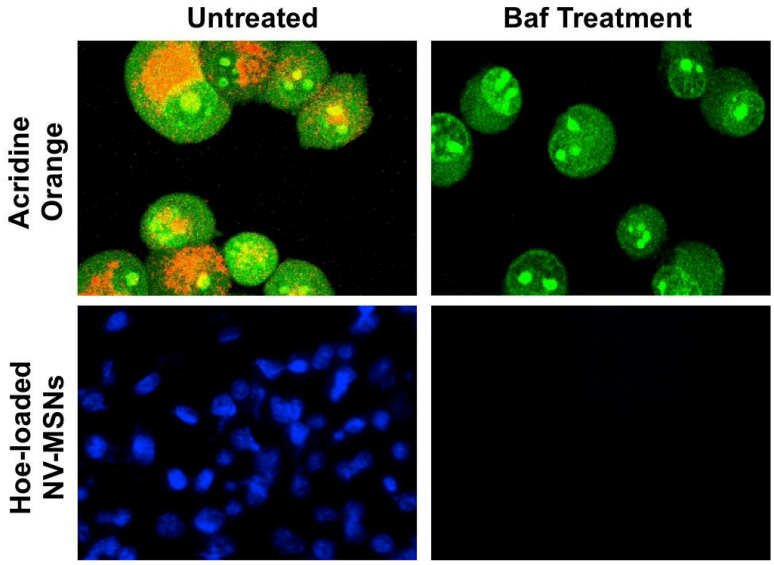

Figure 4.

Cells (green) are treated with acridine orange to detect acidic organelles (orange). Once exposed to Bafilomycin (Baf), the organelles are no longer acidic and no orange fluorescence is seen. Hoechst-loaded NV-MSNs show nuclear staining of cells (blue) but after Baf treatment, the NVs are not activated and no staining is seen.

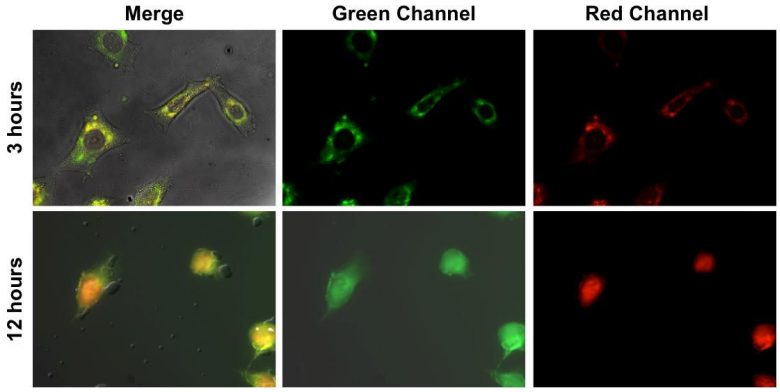

Figure 5.

Confocal images of Dox-loaded MSNs: the green channel represents the MSNs and the red channel shows doxorubicin. At 3 hours, the Dox is contained in the MSNs located inside the cell, but at 12 hours the nanovalves have been activated and the Dox has begun to stain the cell nuclei red.

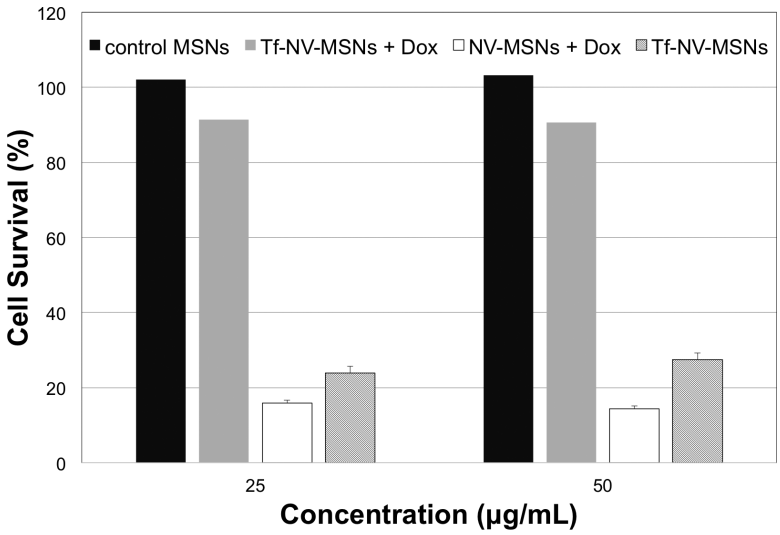

Figure 6.

Cell proliferation assay was carried out with MiaPaCa-2 to observe the efficacy of the Tf-NV-MSN drug delivery system. The MSN-systems without drug did not induce proliferation suppression to cells at all. The Dox-loaded NV-MSNs and the Dox-loaded Tf-NV-MSNs were similarly effective concentrations.

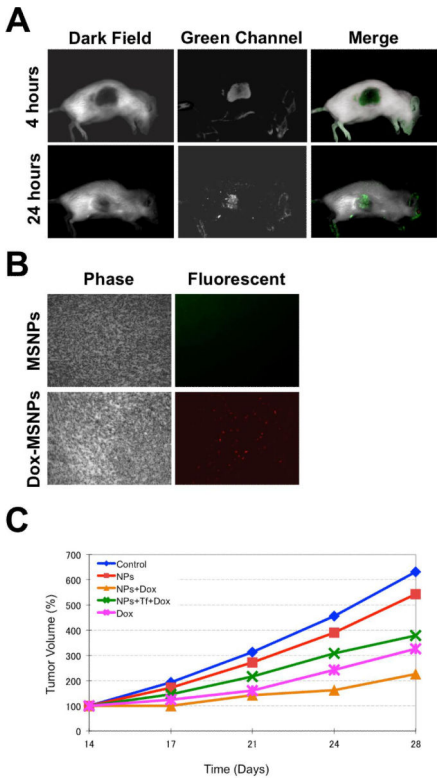

Figure 7.

a) Biodistribution of MSNs in mice with xenograft tumors. SCID mice bearing subcutaneous human pancreatic tumors were injected via tail vein with MSNs. 4 and 24 hours later, the mice were anesthetized, subjected to Maestro 2 *in vivo* imaging system for green fluorescent (MSNs) images. b) Tumors were collected, processed, and analyzed with fluorescence microscope. Red fluorescence indicates doxorubicin in the tumors. c) 25 SCID mice with established xenografts of MiaPaCa-2 were randomly divided to 5 groups (n=5), and the intraperitoneal injections of MSN solutions began once the average tumor diameter reached 3 mm (14^{th} day after inoculation). All injections were done twice per week until the end of the experiment (the 28^{th} day). The average tumor volumes are shown as means ± the standard deviation (SD).